Available online at www.sciencedirect.com

ScienceDirect

Energy Procedia 77 (2015) 565 – 571

Energy Procedia

5th International Conference on Silicon Photovoltaics, SiliconPV 2015

Do lomer dislocations spoil high performance of mc-Si solar cells?

Jan Bauer[a,*], Angelika Hähnel[a], Horst Blumtritt[a], Hakan Deniz[a], Annika Zuschlag[b], Otwin Breitenstein[a]

[a]*Max Planck Institute of Microstructure Physics, Weinberg 2, 06120 Halle, Germany*
[b]*University of Konstanz, Universitätsstr. 10, 78464 Konstanz, Germany*

Abstract

Material induced inherent efficiency losses of multicrystalline silicon solar cells have been investigated across all scales from the solar cell down to the atomic structure of the responsible crystallographic defects. Material inherent efficiency losses can be attributed to local increased dark current, which is found at recombination active small angle grain boundaries and accounts to several per-cent absolute. A one-to-one correlation between the density of Lomer dislocations and the strength of the recombination activity of small angle grain boundaries is found by electron-beam induced current measurements and scanning transmission electron microscope investigations. The increased recombination activity of Lomer dislocations is attributed to their immobile nature, which favors contamination by impurities.

Peer review by the scientific conference committee of SiliconPV 2015 under responsibility of PSE AG

Keywords: efficiency losses; Lomer dislocations; multicrystalline Silicon; dark lock-in thermography; transmission electron microscopy; EBIC

1. Introduction

Regarding the current world market solar cells made from crystalline silicon have a share of about 90 %. From these 90 %, 36 % are distributed to Czochalski (CZ, mono-Si) and approximately 54 % to vertical gradient freeze (VGF, multicrystalline(mc)-Si) silicon, respectively [1]. Assuming that the materials have equal doping levels and undergo the same processes, solar cells made from VGF material show lower performance compared to solar cells made from CZ [2]. VGF material, on the other hand has the advantage of lower costs, mainly due to lower energy

* Corresponding author. Tel.: +49-345-5582761; fax: +49-345-5511223.
E-mail address: jbauer@mpi-halle.mpg.de

Peer review by the scientific conference committee of SiliconPV 2015 under responsibility of PSE AG
doi:10.1016/j.egypro.2015.07.081

consumption [3]. Nowadays the trend goes strongly towards high efficiency solar cells, e.g. passivated emitter and rear cell (PERC) [4,5], and of course industry endeavors to benefit from the advantage of the moderate costs of mc-Si. The main differences of mono-Si and mc-Si are inherent crystallographic defects in mc-Si (which have been discussed exhaustively in literature, see for instance, [6,7]), and higher contamination of mc-Si by metals, e.g. Fe and Cu, and non-metals, e.g. C and N, see [8,9,10]. Successful efforts have been made to develop VGF materials with a high share of mono-Si [11], so called cast-mono, mono-like or quasi-mono, and VGF materials with controlled growth of certain favorable grain boundaries [12], so called high-performance-multi. However, even in these materials still recombination active defects exists. In solar cells the material inherent efficiency losses are mainly attributed to reduction of the carrier lifetime. At some grain boundaries or material defects the lifetime reduction is very strong and causes, besides of a reduction of the short circuit current density, a measureable increased dark recombination current density, also called diffusion current density, described by its saturation current density J_{01}. This dark current is driven by the grade of contamination of the grain boundaries with impurities as well as the type of contamination. Iron is the most prominent "lifetime killer" in mc-Si solar cells.

The impact on solar cell performance of iron, and iron precipitates, and their respective distribution in VGF grown Si blocks was and is still examined by several authors. Nanometer sized iron silicide precipitates have been reported by Buonassisi et al. [13], and have been determined to be the cause of type-II breakdown sites in mc-Si solar cells [14]. The limitation of solar cell efficiency with respect to the iron concentration has been investigated recently e.g. by Schubert et al. [15]. Mainly the iron stems from the quartz crucible and crucible coating, which is made of silicon nitride [16,17]. The impact of the distribution of iron and iron precipitates during the crystallization on cell performance was investigated exhaustively, and it was revealed that especially the material at the edges of Si blocks are affected by the iron contamination [18]. The material induced inherent efficiency losses reported in the above cited literature is always found to be located at so called "grain boundaries", "defects", and "dislocations" of the mc-Si.

Enhanced recombination activity of grain boundaries and other defects in Si was characterized by electron-beam induced current (EBIC) and crystallographic investigations already in the nineteen-eighties. A clear correlation between the EBIC contrast and different dislocation types was made already in 1982 by Pasemann et al. [19], however, the material used in this investigations was CZ grown. Also Kittler et al. showed the recombination activity of dislocations on a model material and found a correlation between EBIC contrast and the contamination level of the dislocations [20]. In mc-Si material it was found that mostly small angle grain boundaries (SAGB) show the strongest EBIC contrast and highest recombination activity [21,22,23]. Seifert and colleagues could reveal in their work a correlation between the density of dislocation and enhanced recombination activity by EBIC measurements [24]. In this work we will try to go further not showing only a one-to-one correlation between dislocations, but revealing the causality between the density of a special type (Lomer) dislocations and local efficiency losses in solar cells made from industrial mc-Si.

2. Experimental

The challenge of the present work is to find exactly the recombination active crystallographic defects having a size of some nm² on a solar cell which is some hundred cm² large. The approach we used is a combination of quantitative dark lock-in thermography (DLIT), scanning- and (scanning) transmission electron microscopy methods (SEM, (S)TEM) and extremely precise, partly in-situ EBIC supported, focused ion beam (FIB) sample preparation. Using these methods in a reasonable manner a one-to-one correlation of the positions of efficiency losses and corresponding crystallographic structures over all scales is possible. For the investigations standard industry screen printed mc-Si solar cells with Al rear contact have been used.

The detection of the position of material induced inherent efficiency losses, i.e. positions with high J_{01}, have been carried out by quantitative DLIT analysis using the Local-IV-2 software [25]. For the local efficiency analyses the global J_{sc} of the cell taken from cell flasher data was used. Identified areas of high J_{01} have been cut out and EBIC investigations have been carried out for high resolution imaging of the defect structure. Using EBIC images small parts of grain boundaries (GBs) showing different EBIC contrast, i.e. different recombination activity, have been cut out with high spatial precision parallel and perpendicular to the solar cell's surface by focused ion beam (FIB). The

resulting FIB lamellas have been thinned down to enable high-resolution imaging of the atomic structure with different STEM methods using a probe C_s-corrected FEI-TITAN 80-300 electron microscope.

3. Diffusion current vs. efficiency evaluation and sample selection

3.1 Diffusion current and efficiency in mono-Si and mc-Si solar cells

Figure 1 illustrates the difference between the diffusion current density (J_{01}) distribution in mono-Si and mc-Si solar cells. In Fig. 1(a) and (b) electroluminescence (EL) images taken at 600 mV of a mono-Si (a) and a mc-Si (b) solar cell are shown. Both images are normalized to the respective maximum signal and are scaled from 0 to 1 in arbitrary units. The EL image of the mono-Si looks much more homogeneous compared to the mc-Si solar cell. Whereas only some dark features due to series resistance effects at interrupted grid fingers are detectable in the mono-Si cell, dark lines in high density are visible in the mc-Si solar cell. Each of these clusters of dark lines, some are exemplarily marked by the white arrows in (b), contains recombination active grain boundaries. In the mc-Si solar cells good areas (black arrows) showing no dark lines, areas with a moderate density of recombination defects (rectangle), and areas with a high density of recombination active defects (circle) can be found.

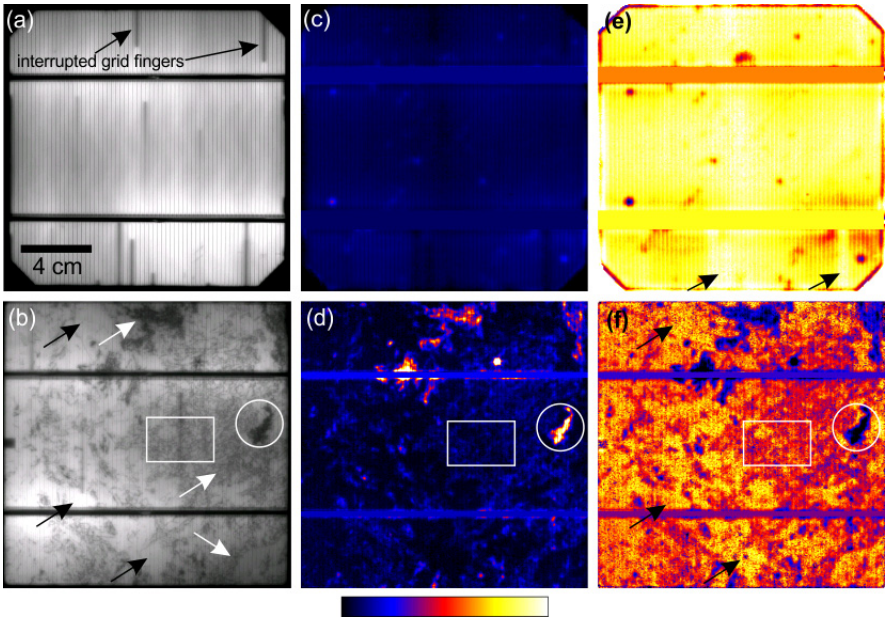

Fig. 1. (a) and (b) are EL images of a mono-Si and a mc-Si solar cell, respectively (scaling 0 to 1 in a.u.). Arrows in (a) denote interrupted grid fingers. Arrows, rectangle, and circle in (b) see text. (c) and (d) are the corresponding DLIT-based J_{01} images (scaling 0 to 2×10^{-11} A/cm²). (e) and (f) are the corresponding simulated efficiency maps (scaling (e): 15 to 18 %, (f): 14 to 17 %). The color bar below the images holds for all scale values given for each picture separately in the text and caption. Length scale in (a) holds for all pictures.

Using the quantitative local current-voltage curve analysis of [25] the J_{01} images of these cells have been obtained and are displayed for the mono-Si cell in Fig. 1(c) and for the mc-Si cell in (d). Both images are scaled form 0 to 2×10^{-11} A/cm², refer to the color scale below the images. At the bus bars a pixel correction is used, which allocates pixel values from the surrounding of the bus bars. This option was used since at the bus bars efficiency losses due the solar cell process are observed (e.g. missing BSF), but here we only want to compare material inherent losses. The mc-Si solar cells shows a very inhomogeneous distribution of J_{01} clusters (bright in Fig. 1(d)), these cluster correlate one-to-one to the dark cluster of the EL image in (b). In the mono-Si such cluster are not detectable. The maximum local J_{01} values are about 5×10^{-10} A/cm² at the mc-Si cell and 5×10^{-12} A/cm² at the mono-Si cell. The simulated efficiency images of both cells in Fig. 1(e) and (f) clearly show that local losses at the J_{01}

cluster account for to 4 % (abs.) in this mc-Si solar cell; the scaling is 15 to 18 % for (e), and 14 to 17 % for (f). Please note, that the cell tester data, i.e. the global efficiency, was measured to be 15.6 % for the mc solar cell and 17.3 % for the mono cell, the simulated data account to 15.7 % and 17.3 %, respectively. Note, also that the resistivity of the material (about 1.5 Ωcm) and series resistance (mono-Si cell: about 0.6 Ωcm² cell, mc-Si cell: 0.7 Ωcm²) of both cells are close to each other, hence the local IV simulations are quite well comparable. However, for simplicity the series resistance was assumed to be homogeneous across the cell area each, which is not correct, but leads only to the artifact of slightly increased efficiency values at the interrupted grid fingers in the simulation of the mono-Si cell, see black arrows in Fig. 1(e). Comparing Fig. 1(d) and (f) it becomes obvious that there is a strong correlation between cluster of high J_{01} and low efficiency. Furthermore, the efficiency distribution of the mono-Si cell is much more homogeneous than that of the mc-Si cell.

3.2 Sample selection

Figure 2(a) shows the simulated J_{01} image of another mc-Si solar cell. Several cluster of increased dark current density J_{01} could be detected and the main cluster was cut out and once again imaged by Local-IV-2 method. The obtained J_{01} image of this small sample is shown in Fig. 2(b). The increased J_{01} is structured in lines and small cluster with areas of very low J_{01} in between. To reveal the efficiency losses at these J_{01} clusters a simulated efficiency map of the sample is given in Fig. 2(c). It is obvious that the efficiency is lower exactly at the position of high J_{01}, where the efficiency was simulated only to be in the range of 12 to 14 % which is about 3 to 5 % lower than the surrounding areas which show efficiencies of up to 17 %. Note that all these efficiency simulations are made under the assumption of electrically isolated pixels, hence these are efficiency potential values. At the right hand side of Fig. 2 a diagram illustrating the dependence of the efficiency on the diffusion current density at the area marked by the circle in Fig. 2(c) is given. The upper efficiency limit follows the relation $\eta \sim \ln(1/J_{01})$; of course the efficiency is affected also by other effects such as increased series resistance or shunting. Recombination current (J_{02}) does not play a role in this area, however the noise of the measurements and subsequent errors in the simulation are present as well and lead to a scatter of the data.

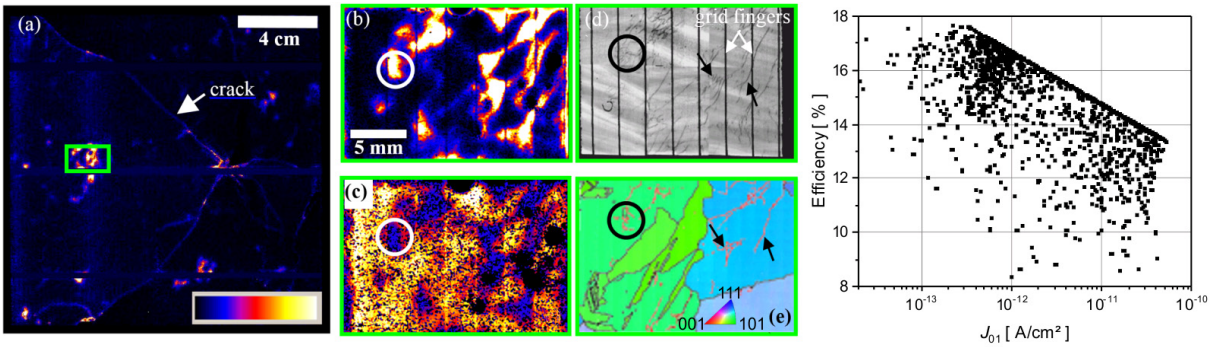

Fig. 2. (a) Simulated DLIT-J_{01} image of a mc-Si solar cell (scaling: 0 to 3.5×10^{-11} A/cm²). The arrow marks a crack, which does not influence the results of the investigations, and is just shown here for the sake of completeness. (b) Simulated DLIT-J_{01} image of the cut out sample (from the rectangle) in the same scale as (a). (c) corresponding simulated efficiency map (scale: 12 to 17 %). (d) stitched EBIC image of the cut out sample. (e) EBSD map of the same position of the direct adjacent wafer. The diagram on the right hand side shows the correlation between J_{01} and efficiency at the position marked by the circle in (c). The color bar in (a) holds for (b), (c) as well referring to the given maximum and minimum values. The length scale in (b) holds for (b) throughout (e).

Using EBIC, images of the cut-out sample were taken and stitched afterwards as shown in Fig. 2(d). The resulting overview clearly demonstrates that the low efficiency areas (i.e. high J_{01}) correlate to lines of low EBIC contrasts, which is exemplarily shown by the black arrows in Fig. 2(d). Due to the EBIC images, which shows a much higher spatial resolution than the DLIT images, it is possible to determine exactly the grain boundaries, which show enhanced J_{01}. To reveal the nature of the grain boundaries forming the grain structure of the sample, an electron backscatter diffraction (EBSD) mapping was done at the same position as the cut out sample on the direct adjacent wafer of the solar cell. The distance between the two wafers is approximately 100 µm, hence we can

assume a very similar grain structure in both samples. The typical inverse pole figure representation of the surface grain orientations is given in Fig. 2(e). The black lines are coincidence site lattice (CSL) grain boundaries, which border the obvious grains with distinct different orientation. The red lines are small angle grain boundaries. By comparing Fig. (d) and (e) it becomes clear that all recombination active structure detected by DLIT and EBIC correspond directly only to small angle grain boundaries (SAGB). The CSL GBs do not show any recombination activity in Fig. 2(d) (see [21,22,23] for comparison). Some of the SAGB are marked by the black arrows and the circle in Fig. 2(e). At the position of the circle a detailed EBIC image was taken, which is given in Fig. 3(a). In Fig. 3(a) some recombination active GBs are visible. It is obvious that the EBIC contrast is different at some GBs and even at one and the same grain boundary the EBIC contrast changes from strong to weak. Four positions with different strong EBIC contrast have been chosen, which are marked in Fig. 3(a), the EBIC contrast decreases from position 1 throughout position 4. Please note that positions 1 and 3, as well as 2 and 4 belong to the same GB, respectively. Exactly at these positions planar, i.e. parallel to the surface, FIB samples have been prepared for subsequent STEM investigation.

4. Electron microscopy investigations of the recombination active structure

To reveal the crystallographic structure of the recombination active grain boundaries, they have been further investigated by high resolution EBIC and STEM. In Fig. 3(b) a superposition of a high magnified EBIC image (in the background) of position 2 and stitched low-angle annular dark field STEM images (LAADF) is shown. At this high magnification the EBIC contrast turns out to be more or less point like, with each point having a different strength.

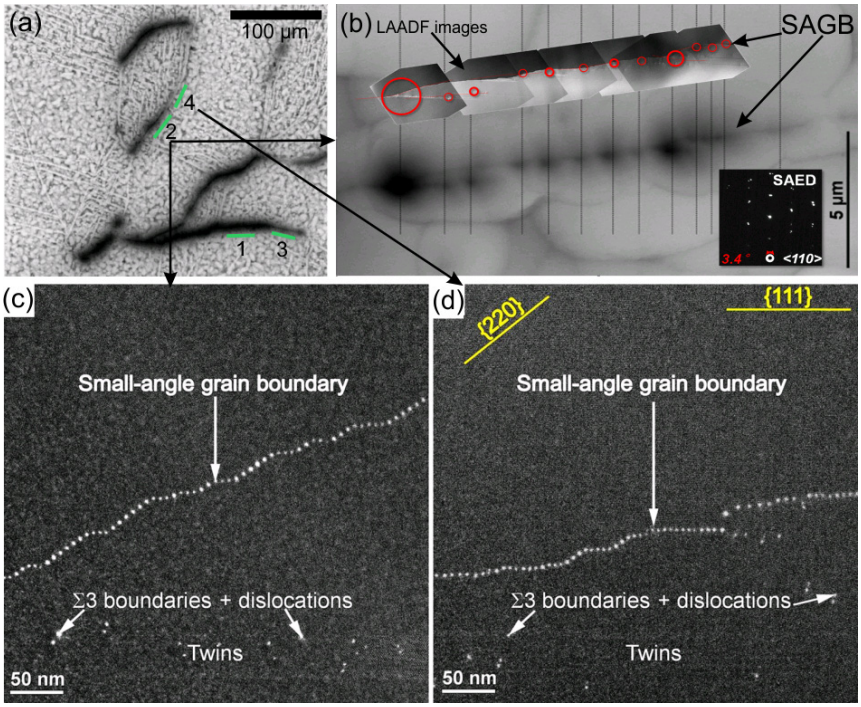

Fig. 3 (a) high resolution EBIC image of the area marked by the circle in Fig. 2(d). (b) Superposition of stitched LAADF images of the small angle grain boundary and a higher magnified EBIC image of position 2. The inset shows a SAED pattern revealing that the grain boundary is a small angle grain boundary. (c) and (d) LAADF-STEM images of position 2 and 4 from (a), respectively.

By comparing the LAADF images, which are located at the correct lateral position in relation to the EBIC image, and the positions of the EBIC events, a clear correlation between the EBIC events and the grain boundary is observed. The red circles at the LAADF images of the GB mark the EBIC events, and their diameter correspond to

the respective strength of the EBIC signal. By selected-area electron diffraction (SAED) the grain boundary was determined to be a small angle grain boundary (SAGB) with a tilt angle of about 3.4° around the <110> direction pointing out of the pattern plane. As demonstrated for that example, also all other investigated grain boundaries with high recombination activity are SAGBs. In Fig. 3(c) and (d) higher magnified LAADF-STEM images of position 2 (c) and of position 4 (d) are shown. At the small angle grain boundaries bright contrasts points are found which are associated with strain fields of partial dislocations and perfect boundary dislocations. It was also found that twin boundaries (Σ3 boundaries) in company with dislocations emanate from the SAGB (see Fig. 3(c),(d)). However, from the EBIC-LAADF comparison of Fig. 3(b) it is clear that only the SAGBs are recombination active. By detailed TEM analysis the perfect boundary dislocations could be identified to be Lomer dislocations. This TEM analyses is not the scope of this contribution and will published elsewhere. By counting the Lomer dislocations and partial dislocations at each of the positions it was found that the density of Lomer dislocations is higher at the high recombination active small angle grain boundaries showing strong EBIC contrast. In Table 1 the EBIC contrast values for each position evaluated from the grey values of the EBIC image in Fig. 3(a) and the density of the Lomer dislocations are listed. The contrast values are average values along the sample size (i.e. approximately at the length of the lines in Fig. 3(a) denoting the positions 1 to 4), and the Lomer dislocation density is the number of Lomer dislocations along the whole small angle grain boundary length, being investigated.

Table 1. EBIC contrast vs. Lomer dislocation density

Position No.	EBIC contrast (%)	Lomer dislocation density (μm^{-1})
1	92 %	100
2	78 %	40
3	68 %	30
4	38 %	7

5. Discussion

The data of Table 1 suggests a clear correlation between the density of Lomer dislocations and the EBIC contrast, i.e. the recombination activity. Though this correlation is evident for our sample it still must be proven by investigating more samples, which is on its way. First results seem to confirm the results shown here. The clear correlation between Lomer dislocation density and EBIC contrast at the SAGBs is a very strong hint that (possibly also pure, undecorated, but at least mostly) Lomer dislocations are detrimental to the performance of mc-Si solar cells. Since Lomer dislocations are immobile, we expect that they are particularly prone for collecting impurities like iron. During our investigation we could not detect any iron in the Lomer dislocation yet. This is due to the fact that the volume we are able to investigate by transmission electron microscopy methods is very small: The TEM lamellas are only about 50 to 100 nm thick and a Lomer dislocation has a typical diameter of about 5 nm. Following the theoretical predictions of Donolato and Kveder et al. [26,27], saying that a density of impurity atoms (iron?) of about 10 μm^{-1} (which is one atom per 100 nm) is enough for strong recombination activity, we expect statistically only one or two iron atoms in the Lomer dislocation regarding the examined volume in our studies. Hence, with the methods used in this contribution it is not possible to detect the iron or other impurity atoms having a similar concentration in the Lomer dislocations.

6. Summary and outlook

Multicrystalline Si solar cells suffer from inherent dark current losses at grain boundaries. The dark current losses could be identified to be located at small angle grain boundaries. Locally the efficiency losses at these SAGB cluster accounts up to approximately 5 % absolute. Furthermore, at the small angle grain boundaries we found a clear correlation between the local density of Lomer dislocations and the recombination activity measured by the EBIC contrast. Other dislocation types found at the same small angle grain boundary do not show significant recombination activity in our investigations. Iron could not be detected yet. By investigating more samples recently

it was confirmed that only the density of Lomer dislocations plays a significant role regarding the recombination activity, which will published elsewhere in greater detail in the near future.

Acknowledgements

The authors acknowledge the help of P. Werner and N. Zakharov (both MPI Halle) at the STEM investigations. This work was partly financed by the BMWi Projects No. 0325270C (SolarWins) and 0325763D (SolarLIFE).

References

[1] Several authors. Photovoltaics Report. www.ise.fraunhofer.de. Freiburg, 24 October 2014. (pdf version downloaded March 2015)
[2] Nijs JF, Szlufcik J, Poortmans J, Sivoththaman S, Mertens RP. Advanced Manufacturing Concepts for Crystalline Silicon Solar Cells. IEEE Transaction Electron Devices 1999;46:1948-1969.
[3] Sirtl E. Future Trends in Solar Silicon Production. Solar Cells 1983;10:101-108.
[4] Blakers AW, Wang A, Milne AM, Zhao J, Green MA. 22.8% efficient silicon solar cell. Appl Phys Lett 1989;55:1363-1365.
[5] Hahn G, Joos S. State-of-the-Art Industrial Crystalline Silicon Solar Cells, Advances in Photovoltaics 2014;3:1-62, in: Semiconductors and Semimetals 90, edited by Willeke GP, Weber ER, Academic Press (Elsevier) London, San Diego, Waltham, Oxford. First Edition 2014.
[6] Wenham SR, Green MA. Silicon solar cells. Prog Photovolt: Res Appl 1996;4:3-33.
[7] Rinio M, Yodyungyong A, Keipert-Colberg S, Borchert D, Montesdeoca-Santana A. Recombination in ingot cast silicon solar cells. Phys Status Solidi A 2011;208:760-768.
[8] Istratov AA, Hieslmair H, Weber ER. Iron contamination in silicon technology. Appl Phys A 2000;70:489-534.
[9] Buonassisi T, Istratov AA, Picket MD, Rakotoniaina JP, Breitenstein O, Marcus MA, Heald SM, Weber ER. Transition metals in photovoltaic-grade ingot-cast multicrystalline silicon: Assessing the role of impurities in silicon nitride crucible lining material. J Cryst Growth 2006;287:402-407.
[10] Søiland AK, Øvrelid EJ, Lohne O, Tuset JK, Engh TA, Gjerstad Ø. Carbon and nitrogen contents and inclusion formation during crystallization of multicrystalline silicon. In: Proc. of the 19th European Photovoltaic Solar Energy Conference, Paris, France 2004;911-914.
[11] Stoddard N, Wu B, Witting I, Wagener M, Park Y, Rozgonyi G, Clark R. Casting Single Crystal Silicon: Novel Defect Profiles from BP Solar's Mono² ™ Wafers. Solid State Phenomena 2008;131-133:1-8.
[12] Zhu D, Ming L, Huang M, Zhang Z, Huang X. Seed-assisted growth of high-quality multi-crystalline silicon in directional solidification. J Cryst Growth 2014;386:52-56.
[13] Buonassisi T, Istratov AA, Peters S, Ballif C, Isenberg J. Imapct of metal silicide precipitate dissolution during rapid thermal processing of multicrystalline silicon solar cells. Appl Phys Lett 2005;87:121918.
[14] Hähnel A, Bauer J, Blumtritt H, Breitenstein O, Lausch D, Kwapil W. Electron microscope verification of prebreakdown-inducing α-$FeSi_2$ needles in multicrystalline silicon solar cells. J Appl Phys 2013;113:044505.
[15] Schubert MC, Kwapil W, Schön J, Habenicht H, Kasemann M, Gundel P, Blazek M, Warta W. Analysis of performance limiting material properties of multicrystalline silicon. Solar Energy Materials & Solar Cells 2010;94:1451-1456.
[16] Schubert MC, Schön J, Schindler F, Kwapil W, Abdollahinia A, Michl B, Riepe S, Schmid C, Schumann M, Meyer S, Warta W. Impact of Impurities From Crucible and Coating on mc-Silicon Quality—the Example of Iron and Cobalt. IEEE J PV 2013;3:1250-1258.
[17] Kwapil W, Zuschlag A, Reis I, Schwirtlich I, Meyer S, Zierer R, Krain Rafael, Kießling FM, Schumann M, Schmid C, Riepe S. Influence of Crucible and Coating on the Contamination of Directionally Solidified Silicon: First results of the German Research Network "SolarWins". In: Proc. of the 27th European Photovoltaic Solar Energy Conference, Frankfurt, Germany, 2012;627-635.
[18] Schindler F, Michl B, Schön J, Kwapil W, Warta W, Schubert MC. Solar cell efficiency losses due to impurities from the crucible in multicrystalline silicon. IEEE J PV 2014;4:122-129.
[19] Pasemann L, Blumtritt H, Gleichmann R. Interpretation of the EBIC Contrast of Dislocations in Silicon. Phys stat sol (a) 1982;70:197-209.
[20] Kittler M, Seifert W, Higgs V. Recombination Activity of Misfit Dislocations in Silicon. Phys stat sol (a) 1993;137:327-335.
[21] Wang ZJ, Tsurekawa S, Ikeda K, Sekiguchi T, Watanabe T. Relationship between electrical activity and grain boundary structural configuration in polycrystalline silicon. Interface Science 1999;7:197-205.
[22] Chen J, Sekiguchi T. Carrier Recombination Activity and Structural Properties of Small-Angle Grain Boundaries in Multicrystalline Silicon. Jap J Appl Phys 2007;46:6489-6497.
[23] Oriwol D, Carl ER, Danilewsky AN, Sylla L, Seifert W, Kittler M, Leipner HS. Small-angle subgrain boundaries emanating from dislocation pile-ups in multicrystalline silicon studied with synchrotron white-beam X-ray topography. Acta Materialia 2013;61:6903-6910.
[24] Seifert W, Morgenstern G, Kittler M. Influence of dislocation density on recombination at grain boundaries in multicrystalline silicon. Semicond Sci Technol 1993;8:1687-1691.
[25] Breitenstein O. Local efficiency analysis of solar cells based on lock-in thermography. Solar Energy Materials & Solar Cells 2012;107:381-389.
[26] Donolato C. Modeling the effect of dislocations on the minority carrier diffusion length of a semiconductor. J Appl Phys 1998;84:2656-2664.
[27] Kveder V, Kittler M, Schröter W. Recombination activity of contaminated dislocations in silicon: A model describing electron-beam-induced current contrast behavior. Phys Rev B 2001;63:115208.